Design of Automatic Controllers for Model-based OPC with Optimal Resist Threshold Determination for Improving Correction Convergence

Yi-Sheng Su, Philip C. W. Ng, Kuen-Yu Tsai, and Yung-Yaw Chen
Department of Electrical Engineering, National Taiwan University, Taipei 106, Taiwan
e-mail: kytsai@cc.ee.ntu.edu.tw, phone: +886-2-33663689

ABSTRACT

Model-based Optical Proximity Correction (MBOPC) has become one of the most important resolution enhancement technologies (RETs), which can effectively improve the image fidelity and process robustness. MBOPC is performed by iteratively shifting the polygon edges of mask patterns until convergence requirements are achieved. In this paper, we specifically discuss the design of feedback controllers to improve MBOPC convergence. Effective controller design rules are derived from the OPC results of several circuit layouts. Meanwhile, resist models also significantly affect MBOPC convergence. Two kinds of resist model have been proposed for MBOPC such as constant threshold resist model (CTRM) and variable threshold resist model (VTRM). We propose a novel CTRM, called pattern-based optimal threshold determination (PBOTD). By normalized mean square error (NMSE) formulation, appropriate threshold values with minimum NMSE can be determined to improve image fidelity, and effectively decrease iterations required. The effectiveness of applying both optimized controller and PBOTD is demonstrated on a 90-nm SRAM cell.

Keywords: Model-based optical proximity correction, resolution enhancement technologies, feedback controllers, constant threshold resist model

1. INTRODUCTION

Due to the continuous shrinkage of lithography wavelength driven by Moore's law [1], optical distortions such as diffraction and proximity effects have become even more serious, which may cause printed patterns distort severely compared with original drawn layouts. Several resolution enhancement technologies (RETs) have been proposed, including phase shifting mask (PSM), optical proximity correction (OPC), off-axis illumination (OAI), and so on. Since the mask data size has approached several hundred gigabytes for modern deep submicron VLSIs, the computation effort of utilizing these RETs has become a crucial problem. In the correction process, each segment is shifted inward or outward in discrete units with respect to the original drawn layout. Each individual segment cannot be handled independently because of the significant interaction between segments within a specific proximity range due to optical coupling effects. This correction process needs to repeat several times in order to satisfy the convergence requirements. In addition, optical model simulation required in each iteration has significant complexity. Hence, the correction is very time consuming that may increase total tape-out cost and time to market. As a result, it is important to reduce the required number of iterations.

In [11], OPC was performed by iteratively shifting the segments with some fixed step size. The fixed step size usually results in slow convergence. One solution to improve the convergence speed is by introducing a proportional damping factor to speed up the process [9]. From classical feedback control's point of view, the damping factor can be treated by tuning the proportional (P) controller. Integral (I) and derivative (D) controllers are other two useful controllers to improve the system dynamic response and steady-state error [8]. The pioneering work in [9] related classical PID control theory to OPC technology. The P, PI, and PID controllers have been applied to improve OPC convergence. However, in this work, only a few locations of segment are chosen to examine the effectiveness of P, PI, and PID controllers. It does not conclude a rule or guideline to help design the controllers to improve the convergence. Our work is intended to extend this approach by heuristically tuning PID parameters for many different patterns. After the tuning process, utilizable design rules for controller parameters can be summarized.

Furthermore, resist models are also important for MBOPC convergence. They are used to describe the behavior of complex chemical interactions and reactions. Two kinds of resist model have been proposed including CTRM and

Optical Microlithography XXI, edited by Harry J. Levinson, Mircea V. Dusa,
Proc. of SPIE Vol. 6924, 69243Z, (2008) · 0277-786X/08/$18 · doi: 10.1117/12.772397

VTRM [10]. CTRM means the area with optical intensity above a certain threshold value will be developed. The selection of threshold value is an important issue because it significant affects the fidelity of printed wafer patterns. We propose a PBOTD approach to facilitate the optimal resist threshold determination. We found that by combining both approaches, significant reduction of number of iterations is possible. The effectiveness of our methodology is tested on two critical layers of a practical 90-nm SRAM cell.

2. MBOPC FLOW AND OVERALL BLOCK DIAGRAM

Fig. 1 depicts the MBOPC flow. A designed layout in CIF format is converted into the internal formats of the MBOPC tool. Number of iterations and dissection length for corrections are determined for following steps. Segmentation of polygons is performed based on the designated dissection length to form small segments along polygon edges, and a target point is assigned for each segment. An optical model is used to simulate the aerial images and a specific threshold value was determined via CTRM to delineate predicted wafer patterns. Edge placement error (EPE) for each segment is evaluated from desired wafer patterns and predicted wafer patterns. The corrections complete when the EPE of each segment falls within a predetermined tolerance. A sophisticated way of correcting each segment is to adjust the amount of edge shift continuously based on our control algorithm. The corrections will cease if the predefined number of iterations is achieved. After the correction process completes, a post-MBOPC layout in CIF format is streamed out after the layout figure is updated. The total MBOPC processing time is proportional to the required number of iterations.

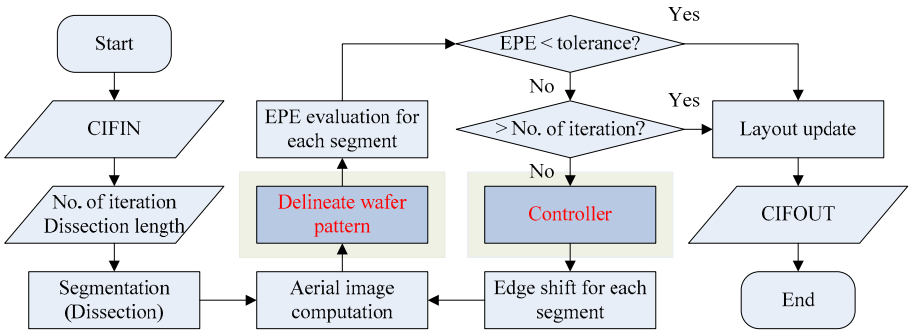

Fig. 1. MBOPC flow

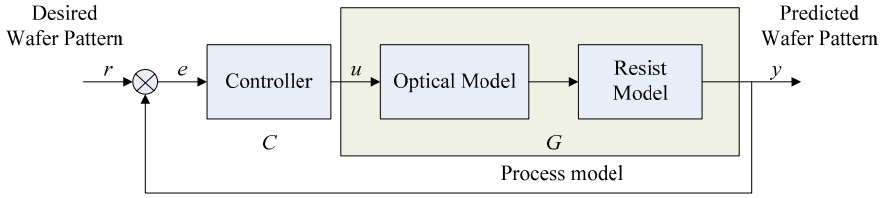

Fig. 2. Overall MBOPC block diagram

Skeleton MBOPC Algorithm:
WHILE (a predefined number of iterations)

(a) Compute intensity for full simulation range.
(b) Evaluate the error between desired wafer patterns and printed wafer patterns for all target points.
(c) Compute the amount of movement for each segment.
(d) Construct a new corrected mask pattern.

END loop

Based on control theories, the convergence properties of our proposed MBOPC flow can be analyzed by a feedback control block diagram shown in Fig. 2. The process model includes an optical model and a resist model. The feedback controller can be a classical P, PI, or PID controller. A heuristic approach for tuning the controller parameters to achieve the convergence requirement is proposed with details explained in Section 2.2 and 2.3. The variables in Fig. 2 are as follows:

(a) r: desired wafer pattern.
(b) y: wafer pattern, the output of the process model.

(c) e: the difference between the wafer pattern and the desired wafer pattern.
(d) C: feedback controller, which is a PID controller.
(e) G: process model, including an optical model and a resist model.

Some preliminary works are necessary to facilitate the MBOPC work. First, the edge dissection length is chosen to maximize correction accuracy while minimizing mask complexity. In general, very aggressive corrections use dissection length of 0.25 to 0.35 exposure wavelength, while dissection length of 0.4 to 0.8 exposure wavelength is used for the more relaxed corrections. Then, overall correction target is assigned for the MBOPC process, which is referred as interpretation filtering in [9]. The EPE tolerance is set to ±5 nm throughout this work.

2.1 Optical Model

Imaging systems are often categorized by the type of illumination scheme. Particularly, illumination coherence can significantly affect the image quality. A broad categorization of illumination schemes is coherent, incoherent, and partially coherent. In lithography imaging, a partially coherent illumination scheme referred as Kohler's illumination as shown in Fig. 3 is commonly utilized. Its mathematical model can be represented by a nonlinear integral equation often referred as the famous Hopkins' model [2].

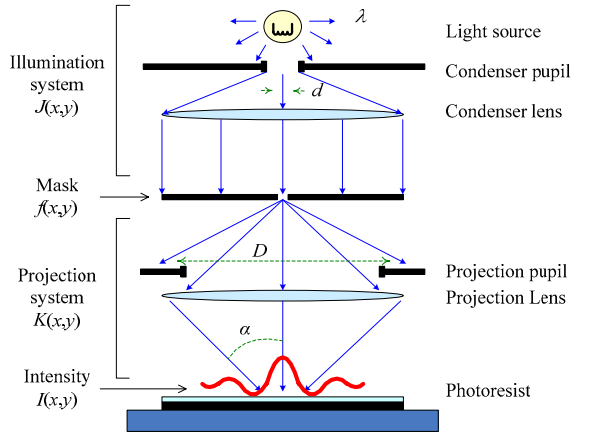

$$
\begin{aligned}
I(x,y) &= \left|g(x,y)\right|^2 \\
&= [T(f)](x,y) \\
&= \int_{\mathbb{R}^4} f(\xi_1,\xi_2) J_0(\xi_1,\xi_2,\eta_1,\eta_2) f^*(\eta_1,\eta_2) \\
&\quad K(x,y,\xi_1,\xi_2) K^*(x,y,\xi_1,\xi_2) d\xi_1 d\xi_2 d\eta_1 d\eta_2
\end{aligned}
\tag{1}
$$

where,
$I(*)$: intensity image at the image plane,
$g(*)$: amplitude image at the image plane,
$f(*)$: object being imaged (mask),
$K(*)$: coherent point spread function,
$J_0(*)$: mutual intensity function.

Fig. 3. Simplified scheme of the typical optical projection system [2]

In this work, dense simulation is utilized to numerically compute the intensity from Eq. (1) at full 2D grid at once [10], based on discrete-time Fourier transforms [3].

2.2 Feedback Controller

Well-known Laplace or Fourier transform were the dominate methods for classical controller design until about 1960. Standard references such as [8] have detailed description of the design of classical PID and lead-lag controllers. The PID control structure has been widely used in industrial control. The advantage of PID control is its low cost and ease of implementation. Moreover, PID control can deal with system transients and steady-state responses. The proportional feedback control (P) can reduce error responses to disturbances but a nonzero steady-state error to constant inputs may remain. The controller with a term proportional to the integral of error (I) can eliminate the steady-state error. Adding a term proportional to the derivative of the error (D) can often improve the transient response. Combining these three terms leads to the classical PID controller.

When applying the PID control to MBOPC, the convergence and the tuning of PID parameters are two important issues. For example, if the derivative term is mistuned, it may cause excessive overshoot of the system transient response. If the integral term is not appropriate, it may lead to system oscillation or instability. Most turning rules of the PID controllers are heuristic. The most famous rule is Ziegler-Nichols tuning [8]. However, it is hardly implemented for multiple-input-multiple-output (MIMO) systems. MBOPC belongs to MIMO systems since it adjusts numerous layout edges to affect numerous target point locations.

We study the convergence and number iterations with respect to the PID parameters on several circuit layouts such as pattern corners, line-ends, and one-dimensional edges. The parameters are tuned heuristically to make the number of required iterations for convergence as small as possible. The experiences gained can be summarized to derive our

heuristic PID tuning rules specifically for MBOPC. As an example, the inverter circuit of Fig. 4 is taken to examine the PID tuning rules. The illumination settings are as follows: (a) wavelength is 193 nm, (b) illumination shape is disk, (c) no aberration and defocus, (d) numerical aperture (NA) is 0.7, and (e) coherent factor is 0.82. These are common values for 90-nm logic processes.

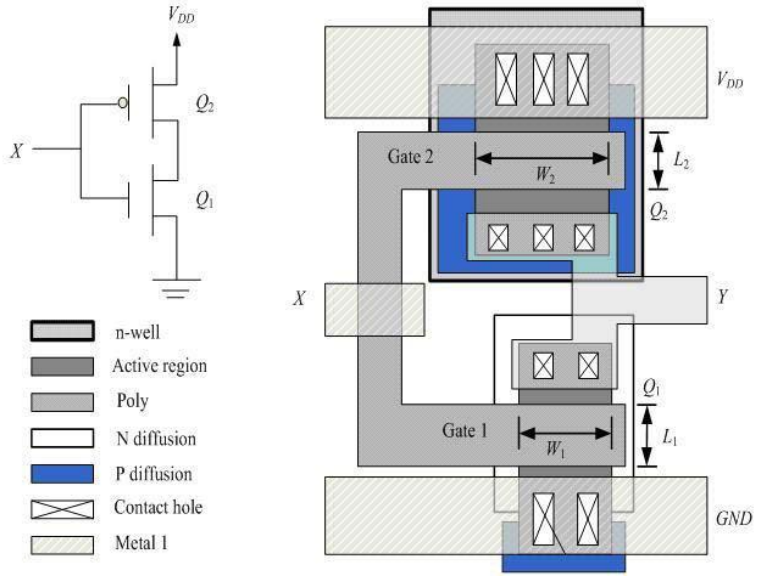

Fig. 4. CMOS inverter and its layout [5]

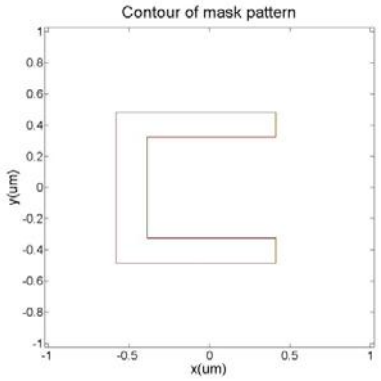

Fig. 5. Contour of mask pattern of polygate

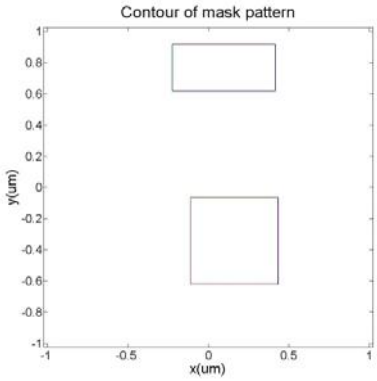

Fig. 6. Contour of mask pattern of N diffusion

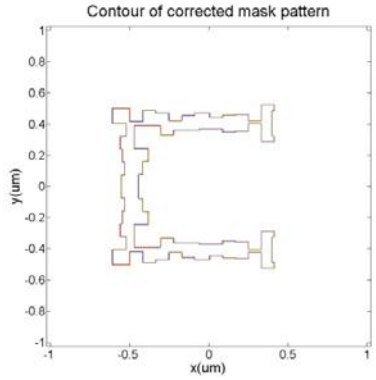

Fig. 7. Contour of aggressive correction mask pattern of polygate

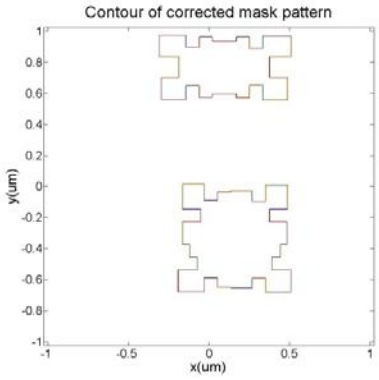

Fig. 8. Contour of corrected mask pattern of N diffusion

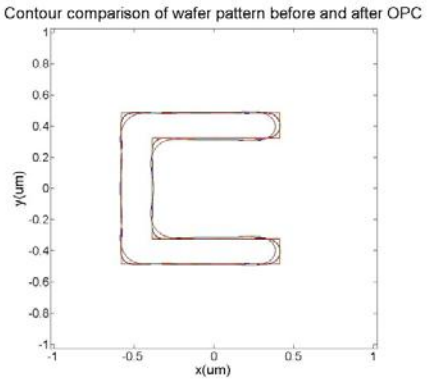

Fig. 9. Contour comparison of wafer pattern of polygate before and after OPC

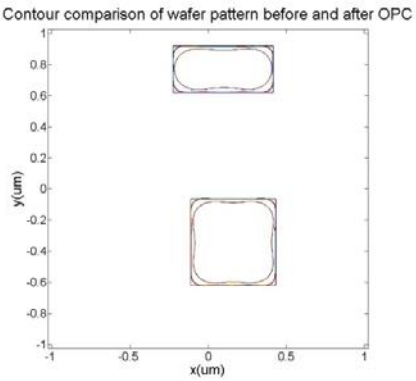

Fig. 10. Contour comparison of wafer pattern of N diffusion before and after OPC

Table 1.PID parameters and needed iteration number for convergence for polygate

P controller	Iteration number	PI controller		Iteration number	PID controller			Iteration number
		P	I		P	I	D	
0.07	30	0.01	0.47	14	0.03	0.15	0.09	30
0.08	30	0.02	0.47	18	0.03	0.26	0.01	28
0.16	30	0.23	0.47	11	0.03	0.28	0.08	24
0.23	30	0.25	0.47	30	0.03	0.31	0.13	30
0.27	30	0.23	0.02	30	0.03	0.54	0.15	30
0.28	30	0.23	0.14	30	0.04	0.01	0.06	30
0.4	30	0.02	0.26	26	0.04	0.24	0.09	30
0.49	30	0.02	0.6	18	0.04	0.43	0.01	24
0.55	30	0.25	0.23	30	0.04	0.46	0.02	22
0.67	30	0.25	0.28	30	0.04	0.53	0.11	30

Table 2.PID parameters and needed iteration number for convergence for N diffusion

P controller	Iteration number	PI controller		Iteration number	PID controller			Iteration number
		P	I		P	I	D	
0.03	30	0.18	0.69	9	0.14	0.35	0.08	17
0.05	30	0.18	0.66	11	0.14	0.28	0.11	23
0.08	30	0.18	0.52	15	0.14	0.26	0.04	26
0.09	30	0.18	0.1	30	0.14	0.08	0.02	30
0.16	30	0.18	0.72	9	0.14	0.38	0.08	19
0.18	30	0.18	0.78	10	0.14	0.41	0.08	18
0.23	30	0.15	0.72	30	0.14	0.45	0.08	16
0.26	30	0.21	0.72	11	0.14	0.45	0.12	18
0.29	30	0.24	0.72	9	0.14	0.45	0.15	21
0.35	30	0.18	0.81	9	0.14	0.45	0.2	30

2.3 Brief Summary of PID Tuning for MBOPC

Table 1 and Table 2 show the P, PI, and PID parameters and needed number of iterations for polygate and N diffusion layers. In addition, we performed the tuning process to other layers such as active region, P diffusion, contact hole, metal, and so on, but the results are similar thus not shown. Our findings and heuristic tuning rules are summarized as below:

A. P Controller

- If the gain of P controllers is too small, there is nonzero steady-state error. On the other hand, if the gain of P controllers is too large, the system response will oscillate.

B. PI Controller

- I controllers may effectively decrease the error and improve the convergence.
- The system response is sensitive to the P controller parameter. A small change of P controllers may affect the system convergence.
- *The recommended tuning rule is that the parameter values of P controllers and I controllers are between zero and one.*

C. PID Controller

- Adding derivative terms to PI controllers usually does not change convergence drastically.
- *The recommended tuning rule is that the parameter values of P controllers, I controllers, and D controllers are between zero and one*.

2.4 Constant Threshold Resist Model

To determine the developed wafer patterns, a simple approach is to treat the resist as a threshold detector. The threshold detector can be thought of as a zero-order approximation of resist responses. Based on CTRM, only areas with intensity above a certain value are developed. This resist model is commonly used to fast predict printed wafer patterns. There are two different threshold determinations explained as follows:

A. Grating-based Optimal Threshold Determination

As shown in Fig. 11, the aerial image of a dense-line mask pattern generated by the lithography simulator is used to determine an appropriate threshold level. Both line space and line width of the layout are 90 nm. With a threshold value of 0.29, the resolved critical dimension of the center line is close to 90 nm. This approach, called grating-based optimal threshold determination (GBOTD), is suitable for random logic since polygate linewidth control is usually the key lithography objective.

B. Pattern-based Optimal Threshold Determination

We propose a novel approach called pattern-based optimal threshold determination (PBOTD). Appropriate threshold values are selected by normalized mean square error (NMSE) formulation. NMSE is defined for a quantitative measure of the differences between two computed images:

$$NMSE(\mathbf{A},\mathbf{B}) = \frac{\sum_{i=1}^{n}\sum_{j=1}^{m}\left|a_{ij}-b_{ij}\right|^2}{\sum_{i=1}^{n}\sum_{j=1}^{m}\left|a_{ij}\right|^2} \tag{2}$$

where the matrices *A* and *B* represent the two images to be compared for the same circuit layout. Thus the relative error between desired wafer patterns and predicted wafer patterns can be calculated. Appropriate threshold values with minimum NSME are chosen to improve image fidelity, and effectively decrease iterations by providing the MBOPC a better initial condition. Poly and active layers of a 90-nm 6-T SRAM cell [13] are examined. Fig. 12 illustrates a novel resist threshold determination for both layers, where a threshold value of 0.23 leads to small NMSE for both layers. This approach is appropriate for periodic patterns such as memory cells in view of linewidth control of the entire layout for manufacturing yield.

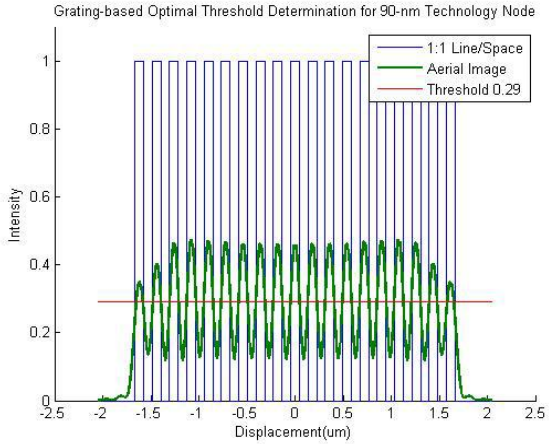

Fig. 11. Grating-based optimal threshold determination for 90-nm technology node

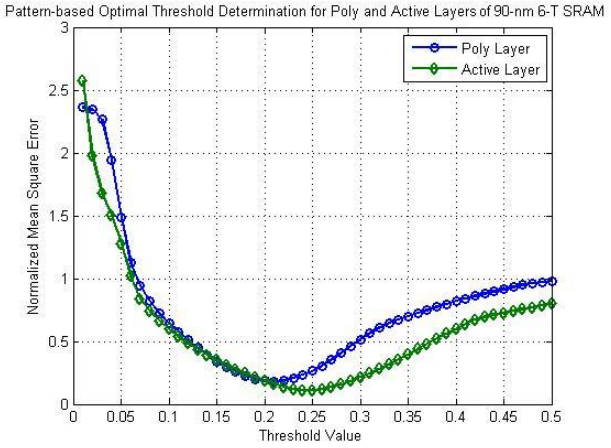

Fig. 12. Pattern-based optimal threshold determination for the poly and the active layers of a 90-nm 6-T SRAM cell

3. SIMULATION RESULTS AND DISCUSSION

Our aerial image simulator is based on two-dimensional Fast Fourier Transforms (FFT). By utilizing FFT, it is implied that the mask layout is 2-D periodic [3][13]. Therefore, the simulation of a set of four 6-T SRAM cells is required as shown in Fig. 19 and Fig. 21, where they are the smallest patterns duplicated on the mask (simulation range: 1.388 μm × 3.320 μm). In the correction processes, each edge of poly and active patterns is dissected into 30-nm segments. Based on the proposed heuristic tuning rule, the PID controller parameters are set to 0.05, 0.08, and 0.01 respectively. To analyze the correction performance with two different resist threshold determinations, MBOPC is executed with the number of iterations from 0 to 20. Fig. 13 and Fig. 14 show NSME versus number of iterations for poly and active layers using both GBOTD and PBOTD approaches with a gradual reduction. But the initial NMSE in poly layer is manifestly greater than active layer. By optimizing the threshold value using PBOTD approach, the initial NMSE in both layers are significantly reduced. For example, by considering the 11th segment, Fig. 16 and Fig. 18 clearly show that EPE for the poly and the active layers using PBOTD approach has quickly fallen within a predetermined tolerance compared to GBOTD approach in Fig. 15 and Fig. 17 respectively. In summary, PBOTD approach can substantially improve the convergence speed of

MBOPC as shown in Table 5. The speed of convergence by using PBOTD approach for both layers is about 400% improvement compared to GBOTB. After 20 iterations using PBOTD approach, the corrected poly and active mask patterns are illustrated in Fig. 20 and Fig. 22.

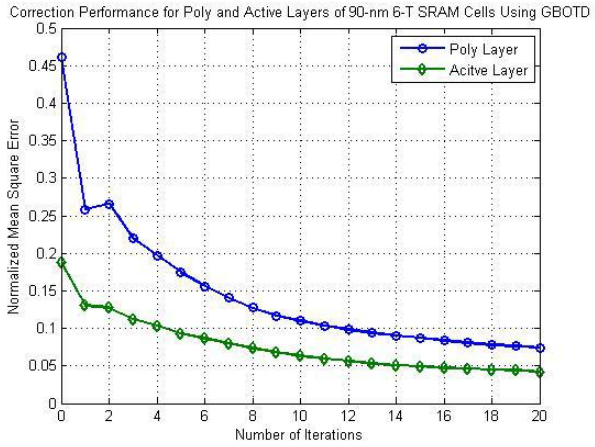

Fig. 13. Correction performance for the poly and active layers using GBOTD approach

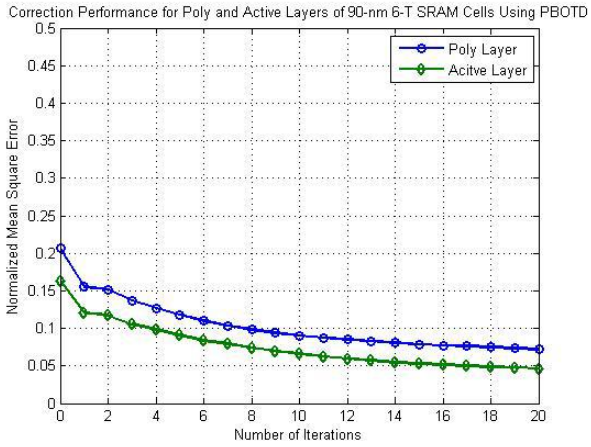

Fig. 14. Correction performance for the poly and active layers using PBOTD approach

Table 3.NMSE vs. number of iterations for the poly and active layers using GBOTD approach

ITER. NO. / NMSE	0	5	10	20
Poly Layer	0.4619	0.1746	0.1098	0.0742
Active Layer	0.1881	0.0931	0.0632	0.0420

Table 4. NMSE vs. number of iterations for the poly and active layers using PBOTD approach

ITER. NO. / NMSE	0	5	10	20
Poly Layer	0.2064	0.1183	0.0904	0.0719
Active Layer	0.1634	0.0910	0.0660	0.0464

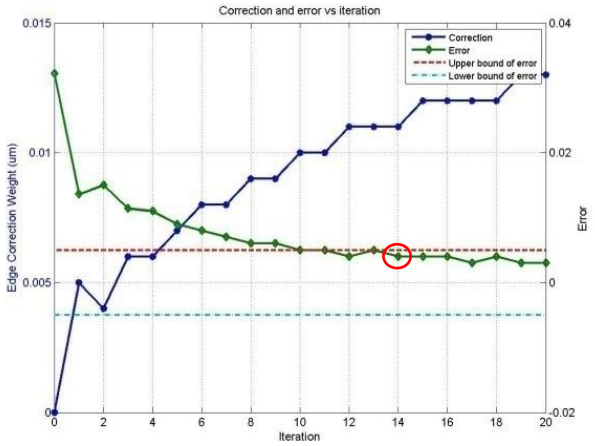

Fig. 15. Correction and error vs. number of iterations for the 11th segment of the poly layer using GBOTD approach

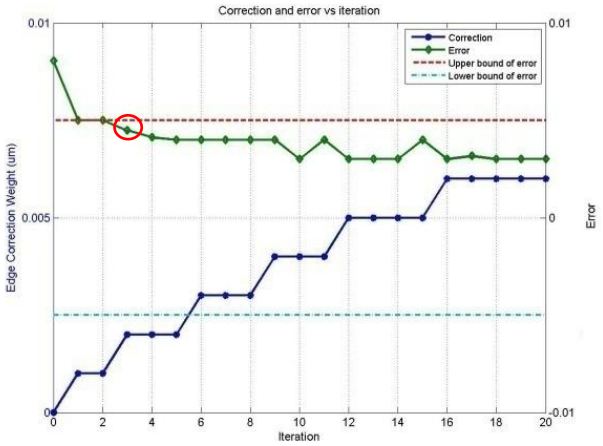

Fig. 16. Correction and error vs. number of iterations for the 11th segment of the poly layer using PBOTD approach

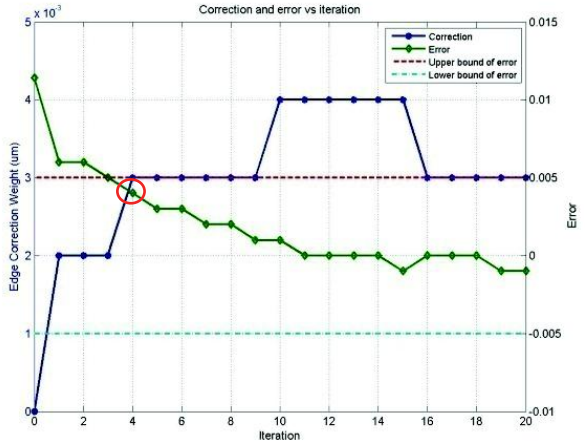

Fig. 17. Correction and error vs. number of iterations for the 11th segment of the active layer using GBOTD

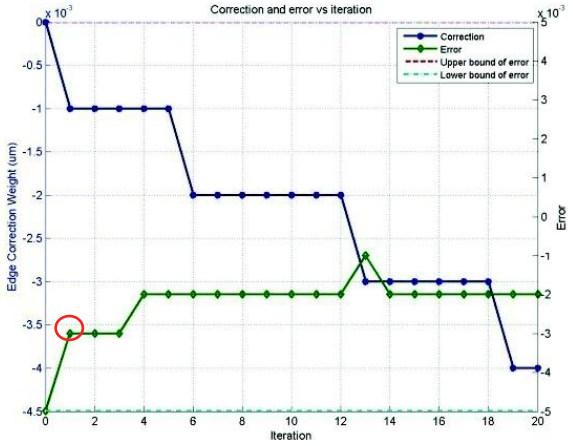

Fig. 18. Correction and error vs. number of iterations for the 11th segment of the active layer using PBOTD approach

Table 5.Comparison of convergent iteration number for the 11th segment of the poly and active layers using GBOTD and PBOTD approaches

METHOD / CONVERGENT ITER. NO.	GBOTD	PBOTD
11th segment of poly layer	14	3
11th segment of active layer	4	1

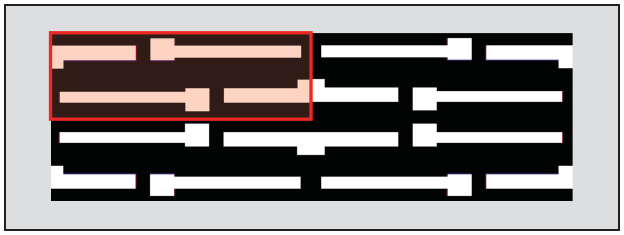

Fig. 19 Poly mask pattern of the 90-nm 6-T SRAM cells

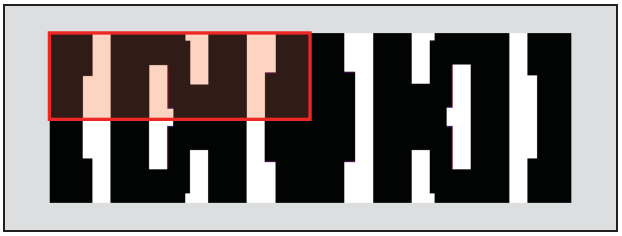

Fig. 21 Active mask pattern of the 90-nm 6-T SRAM cells

Fig. 20 Corrected poly mask pattern of the 90-nm 6-T SRAM cells after 20 iterations using PBOTD approach

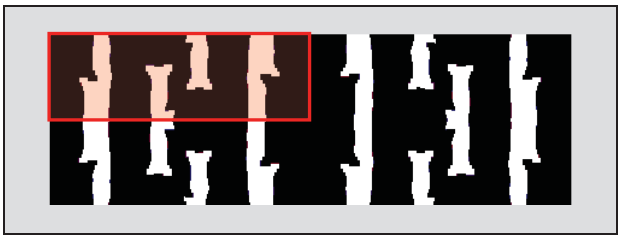

Fig. 22 Corrected active mask pattern of the 90-nm 6-T SRAM cells after 20 iterations using PBOTD approach

4. CONCLUSIONS AND FUTURE WORK

The PID controller can effectively reduce the iteration number as long as the parameters of controller are designed properly. From the results of performing MBOPC on several different layers, useful experiences in tuning the PID parameters have been concluded as a set of heuristic rules and guideline. They could facilitate OPC engineers to quickly acquire feasible controller parameters to achieve required specifications. In addition, PBOTD approach certainly provides a good way to decide the optimal threshold value in order to minimize the initial error before performing MBOPC. An obvious result of combining the advantage of both methodologies is significantly speeding up the

correction process. Additional acceleration could be obtained by adjusting target point locations in accordance with specific layout topologies and design intent. This is under investigation.

5. ACKNOWLEDGEMENT

This work was supported in part by National Science Council of Taiwan and in part by Taiwan Semiconductor Manufacturing Company Limited.

6. REFERENCES

1 G. Moore, "Cramming more components onto integrated circuits," *Electronics*, 38(8), (1965).
2 Y. C. Pati, A. A. Ghazanfarian, and R. F. Pease, "Exploiting structure in fast aerial image computation for integrated circuit patterns," *IEEE Trans. on Semiconductor Manufacturing*, 10(1), (1997).
3 A. V. Oppenheim and R. W. Schafer*, Discrete-time Signal Processing*, 2nd ed., Prentice Hall, 1998.
4 N. B. Cobb, Fast Optical and Process Proximity Correction Algorithms for Integrated Circuit Manufacturing, PhD dissertation, Berkeley University, 1998.
5 A. S. Sedra, K. C. Smith, *Microelectronic Circuit*, 4th ed., Oxford University Press, 1998.
6 ITRS, 2001 lithography roadmap optical mask requirements, http://public.itrs.net/Files/2001ITRS/Home.htm
7 M. L. Rieger, V. Gravoulet, J. Mayhew, D. Beale, R. Lugg, "Enriching Design Intent for Optimal OPC and RET", *Proc. SPIE*, 4754, 132-137, (2002).
8 G. F. Franklin, J. D. Powell, A. E. Naeini, *Feedback Control of Dynamic System*, 4th ed., Addison Wesley, 2002.
9 B. Painter, L.S.M. III, M.L. Rieger, "Classical Control Theory Applied to OPC Correction Segment Convergence," *Proc. SPIE*, 5377, 1198-1206, (2004).
10 W. C. Huang, C. H. Lin, C. C. Kuo, C. C. Huang, J. F. Lin, J. H. Chen, R. G. Liu, Y. C. Ku, and B. J. Lin, "Two threshold resist models for optical proximity correction," *Proc. SPIE*, 5853, (2005).
11 N. Cobb, "Flexible sparse and dense OPC algorithms," *Proc. SPIE*, 5853, (2005).
12 W. C. Huang, C. M. Lai, B. Luo, C. K. Tsai, M. H. Chih, C. W. Lai, C. C. Kuo, R. G. Liu, and H. T. Lin, "Intelligent model-based OPC," *Proc. SPIE*, 6154, (2006).
13 M. F. You, Philip CW Ng, Y. S. Su, K. Y. Tsai and Y. C. Lu., "Impact of optical correction settings on electrical performances," *Proc. SPIE*, 6521, (2007).